Vietnam Journal of Earth Sciences, 43(4), 524-545, https://doi.org/10.15625/2615-9783/16572

Vietnam Academy of Science and Technology
Vietnam Journal of Earth Sciences
http://www.vjs.ac.vn/index.php/jse

Geochemistry and mineralogy of the Truc Thon Clay, Hai Duong Province, North Vietnam: implication for paleoclimatic and provenance analysis

Hoang Van Tha[1*], Shahid Iqbal[2*], Urszula Czarniecka[3], Anna Wysocka[4], Phan Dong Pha[5], Nguyen Quoc Cuong[1], Vu Van Ha[1], Dang Minh Tuan[1]

[1]*Institute of Geological Sciences, VAST, Hanoi, Vietnam*
[2]*Department of Earth Sciences, Quaid-i-Azam University, Islamabad, 45320, Pakistan*
[3]*Department of Geosciences, University of Oslo, P.O Box 1047 Blindern, 0316 Oslo, Norway*
[4]*Faculty of Geology, University of Warsaw, Żwirki i Wigury 93, Warsaw, Poland*
[5]*Institute of Marine Geology and Geophysics, VAST, Hanoi, Vietnam*

Received 15 July 2021; Received in revised form 09 September 2021; Accepted 13 October 2021

ABSTRACT

During the Miocene-Pleistocene, generally sub-tropical to tropical warm and humid paleoclimate prevailed in Southeast Asia with a gradual cooling trend. The Truc Thon clay (TTC) mine presents interesting outcrops for sedimentological and provenance analysis. The present study uses results of geological investigation in 16 outcrops and wells at the clay mine Truc Thon. The TTC has lens-shaped geometry, filled with two clay bodies, including grey-white clay and multicolor clay. Bulk mineralogy indicates the predominance of quartz and a relatively high amount of pyrophyllite. Clay mineralogy shows the presence of main kaolinite, followed by illite and mixed-layer illite-smectite. These may interpret a warm, humid paleoclimatic condition in the source areas. Illite may be inherited from basement rocks. The bulk rock geochemistry supports intense chemical weathering with the Chemical Index of Alteration (CIA) in the TTC ranged ca. 80.6-98 (average = 90.4). In combination with the geochemical proxies and the mineralogical composition of the TTC, the chemical weathering intensity indicated warm/hot, semi-humid/humid tropical paleoclimate in the source area. A combination of mineralogical and geochemical analyses with regional geological features show that the Hon Gai Triassic rocks are the main source for the TTC. Source materials are originally related to silicic rocks of granitic-granodioritic composition. Paleoclimatic conditions favored intense chemical weathering of the Hon Gai Triassic rocks and surrounding rocks, creating a ceramic mine of great industrial value.

Keywords: Truc Thon clay; bulk-rock geochemistry; clay mineralogy; paleoclimate; provenance.

1. Introduction

In recent years, there have been many attempts to reconstruct the evolution of the Southeast Asian Monsoon during the Cenozoic. The scientific data of paleoclimatic conditions have been evidenced in Vietnam during the Oligocene (Böhme et al., 2010; Wysocka et al., 2020; Song et al., 2021). A

*Corresponding author, Email: thahoangvan@gmail.com

warm and humid climate was recorded for the Oligocene (Böhme et al., 2010; Song et al., 2021). According to Zachos et al., 2001, the Cenozoic has been noticed by long-term global cooling, culminating in the Pleistocene ice ages. Global deep-sea oxygen and carbon isotope records clearly represented gradually cooling from the Mid-Miocene to Pleistocene (Zachos et al., 2001). During the Pleistocene, the climate shifted in response to the prevailing glacial-interglacial cycles. Dry-cool paleoclimate occurred during the glacial followed by warm-humid climate during the interglacials (Bahlburg and Dobrzinski, 2011). One of the most important topics of global concern in recent decades has been climate change (Tuyet et al., 2019; Ly and Thuy, 2019).

The geochemical characteristic of sedimentary rocks is commonly controlled by four main factors, including parent rock composition, prevailing weathering, sediment transport, and diagenesis. Heretofore, several geochemical proxies were built to decipher paleoenvironments, provenance, and paleoclimate (McLennan et al., 1993; Garver et al., 1996; Nesbitt and Young, 1982; Fedo et al.,1995; Roser and Korsch, 1988, Bibi et al., 2019). Geochemical proxies of fine-grained sediments are widely applied in reconstruction for paleoenvironments, alteration and weathering, and provenance (e.g., Hofmann et al., 2001; Cullers, 2002; Cullers and Podkovyrov, 2002; Lee, 2002; Rahman and Suzuki, 2007; Goldberg and Humayun, 2010; Madhavaraju et al., 2010; Hofer et al., 2013; Iqbal et al., 2019).

Vietnam clays have been widely used in daily life, such as making bricks, ceramics, refractory materials, drilling fluid, geopolymer, and peloid, etc. (Ti, 1985; Long, 2006; Lan et al., 2019; Man et al., 2020). The TTC is famous for its ceramic and refractory quality. Therefore, it has remained the focus of interest since the 1960s (Diet, 1975; Ti, 1985; Long, 2006). Both the good data and geochemical composition of clay have focused on the applicability of the TTC for the ceramic industry and refractory materials, but it has neglected the scientific potential. Moreover, there have been no geochemical data to confirm paleoclimatic conditions during the Miocene - Pleistocene in Vietnam. The present study attempts to use geochemical and mineralogical data of the TTC mine to unravel the paleoclimatic conditions and provenance analysis.

2. Geological setting

The TTC mine in Vietnam is located in the Pha Lai-Dong Trieu structural Block, Ke Bao-Dong Trieu Zone of the northeast coal Basin. It is bounded by N 21°06’49.59’’-N 21°08’13.99’’latitude, and E 106°22’46.27’’-E 106°24’58.54’’ longitude (Fig. 1). The basement consists of the Triassic Hon Gai Formation (T_3n-r*hg*). The Hon Gai Formation is divided into three parts, but only the middle and upper parts in the study area (Ky, 1999; Luc, 2017). The middle part is characterized by fine-grain sediments successions such as siltstones, clays, and calcareous claystones, which bear thick coal seams. Sandstones are rich in quartz, but sericite predominates in siltstones, claystones. The presence of calcareous rocks with 53% carbonate indicates a marine geological process during sedimentation. The upper part mainly consists of fluvial coarse-grained compositions such as grey, white-grey conglomerates, and sandstones (Diet, 1975; Luc, 2017). The interbeds are layers or lens of fine-grain sandstones, siltstones, claystones with grey, white-grey, pink, black-grey in color. The rocks are mainly composed of quartz, sericite, and chlorite, clearly observed by thin sections (Diet, 1975). The sedimentary succession of the TTC quarry is mainly composed of clay, silt, sand, and gravel, in which clay accounts for most sediment. The clay quarry and its vicinity consist of three lithostratigraphic units (Ky, 1999), including (1) sand, gravel, silty clay, clay of the Vinh Phuc Formation

(Q_1^3vp), (2) silty clay, sandy silty clay, of the Hai Hung Formation ($Q_2^{1-2}hh$), and (3) silty clay, sandy silt, sand, gravely sand of the Thai Binh Formation (Q_2^3tb) (Fig. 1).

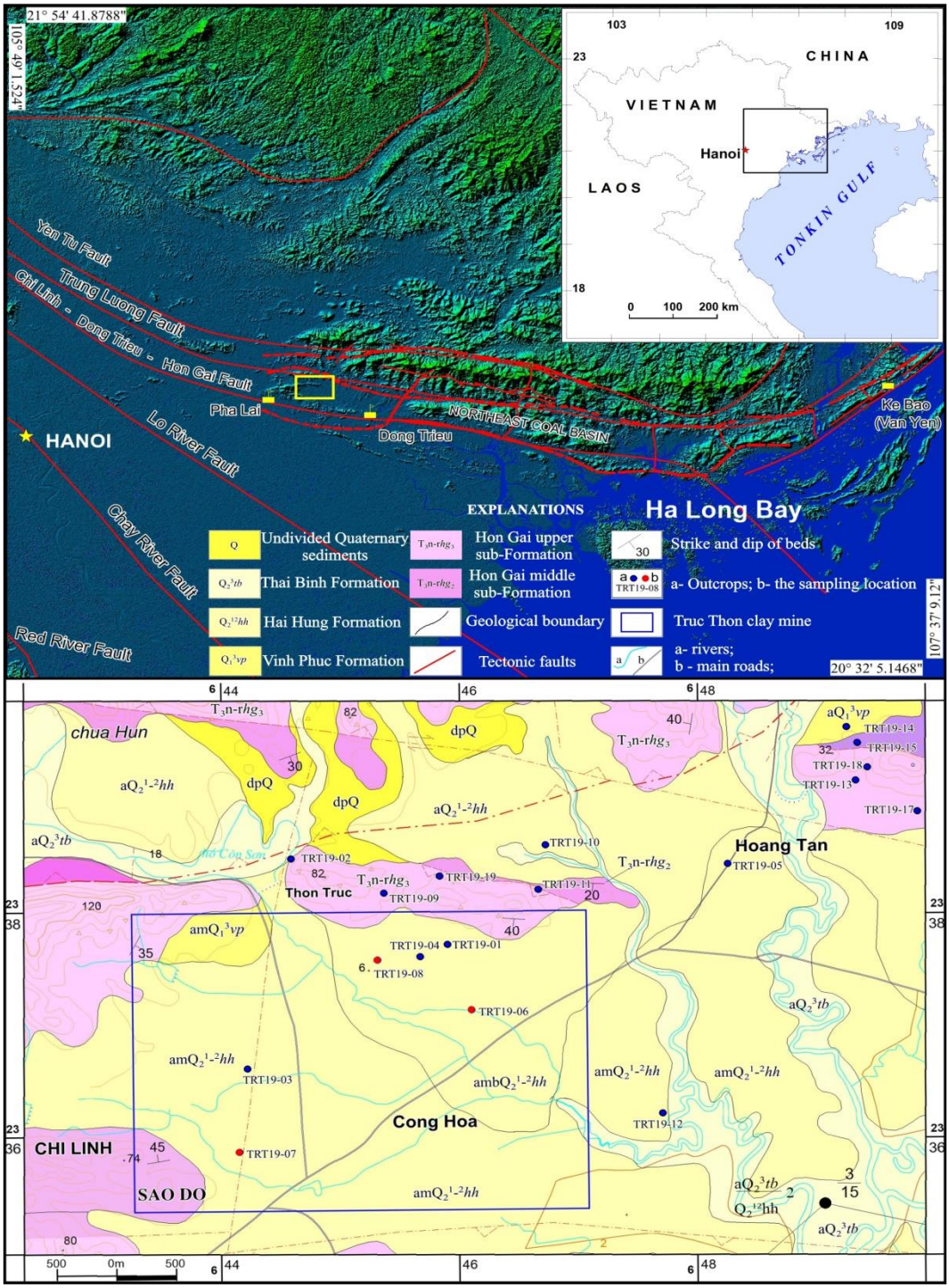

Figure 1. Geological map of the TTC mine and adjacent area (based on Luc, 2017)

The specific scientific evidence to determine the age of the TTC member is still doubted, and some workers considered the TTC to be of the Neogene age (Diet, 1975). Huyen (1996) classified the TTC into the late Pleistocene Vinh Phuc Formation, the same as the point of view of Ky (1999), who established the Hai Phong geological map sheet at the scale of 1:200,000. Therefore, the forming period of the TTC seems to be still debated.

The depositional environment has been mentioned in the geological documents. On the geological map of 1:200,000 scale, the outcrop of the TTC is classified into the Vinh Phuc marine Formation ($mQ_1^3 vp$) (Huyen, 1996; Ky, 1999). On the geological map at a scale of 1:50,000, the exposed area of Truc Thon was classified in fluvio-marine sediments of the Hai Hung Formation ($amQ_2^{1-2} hh$) (Luc, 2017). The interfinger structure is present in the margins of the TTC mine. An association of lithofacies includes massive clay (Fm) and massive mud (Fsm) with 6.5-12 m in thick (TRT19-06/1, TRT19-07, TRT19-08) which are deposited from low suspension falling out in bodies of standing water (Miall, 2006; Tha et al., 2019). Clay mineral composition is typical by an assemblage of kaolinite-chlorite-vermiculite. The TRT19-08 appears some fragments of freshwater diatoms (Prof. Andrey Yu. Gladenkov of the Russian Academy of Science). This evidence reflects the depositional condition of clay in a lake environment (Tha et al., 2019).

3. Materials and methods

The field-based studies were supported by topographic map (scale 1:50,000), and geological maps (scale 1:100,000 and 1:200,000). The field data and samples were gathered at 16 geological exposures (Figs. 1, 2), in which three outcrops were chosen to document detailed data and analyzed samples; 5 samples of bulk mineralogy and 3 samples of clay mineralogy, 7 samples of major elements, and 4 samples of rare earth and trace elements.

Seven bulk geochemical samples were conducted on the TTC: Major oxides, trace, and rare earth elements of two samples were quantified by laser ablation inductively coupled plasma mass spectrometry (LA–ICP–MS) at Bureau Veritas Minerals Laboratories Ltd., Vancouver, Canada (TRT19-08/2, TRT19-08/03; Appendix 1); two samples were tested at the Laboratory of Analytical Chemistry, Institute of Chemistry, Vietnam Academy of Science and Technology (VAST), Vietnam (TRT10-06/1, TRT19-07/1; Appendix 1); three samples were tested for major oxides at the Center for Analytical Laboratories, Institute of Geological Sciences (VAST) (TRT19-08/2a, TRT19-08/03a, TRT19-10; Appendix 2). Besides, 98 well logs and 62 samples of major elements analysis from the projects reports for the TTC mine were included (Ti et al., 1985; Long, 2006; Appendix 2). These samples were collected at different depths from the Truc Thon clay mine (see Fig. 2; Appendix 2).

Five samples were selected for analysis of bulk mineralogy. Powder XRD was used for the determination of the bulk mineralogical composition. Three samples were tested for clay mineralogy by the <2 μm grain-size fraction. XRD analysis was conducted using Empyrean-PAN analytical diffractometer (Cu-Kα- radiation (45 kV, 40 mA), step size 0.026s per step) at the Department of Mineralogy, the Institute of Geological Sciences (VAST).

For reconstruction of paleoclimatic conditions, the Chemical Index of Alteration (CIA) is calculated and establishes relationships with other proxies, such as Al_2O_3, K_2O/Na_2O, Index of Compositional Variability (ICV). Al_2O_3 vs. $CIA_{(molar)}$ and K_2O/Na_2O vs. $CIA_{(molar)}$ plots are used to distinguish between the arid, subtropical, and tropical paleoclimates (Goldberg and Humayun, 2010; Iqbal et al., 2019). SiO_2% vs.

(Al_2O_3+K_2O+Na_2O)% plot is used for determining humidity (Iqbal et al., 2019). The plot of Al_2O_3, CaO*+Na_2O, and K_2O (A-CN-K, Nesbitt, and Young, 1984; Bahlburg and Dobrzinski, 2011) shows the connection between mineralogical compositions and the weathering trends, where CaO* is the amount of CaO incorporated in the silicate fraction of the clay. The other proxies are also supported, such as Chemical Index of Weathering (CIW), Chemical Proxy of Alteration (CPA), Plagioclase Index of Alteration (PIA), ICV, and in combination with the assemblage of clay minerals.

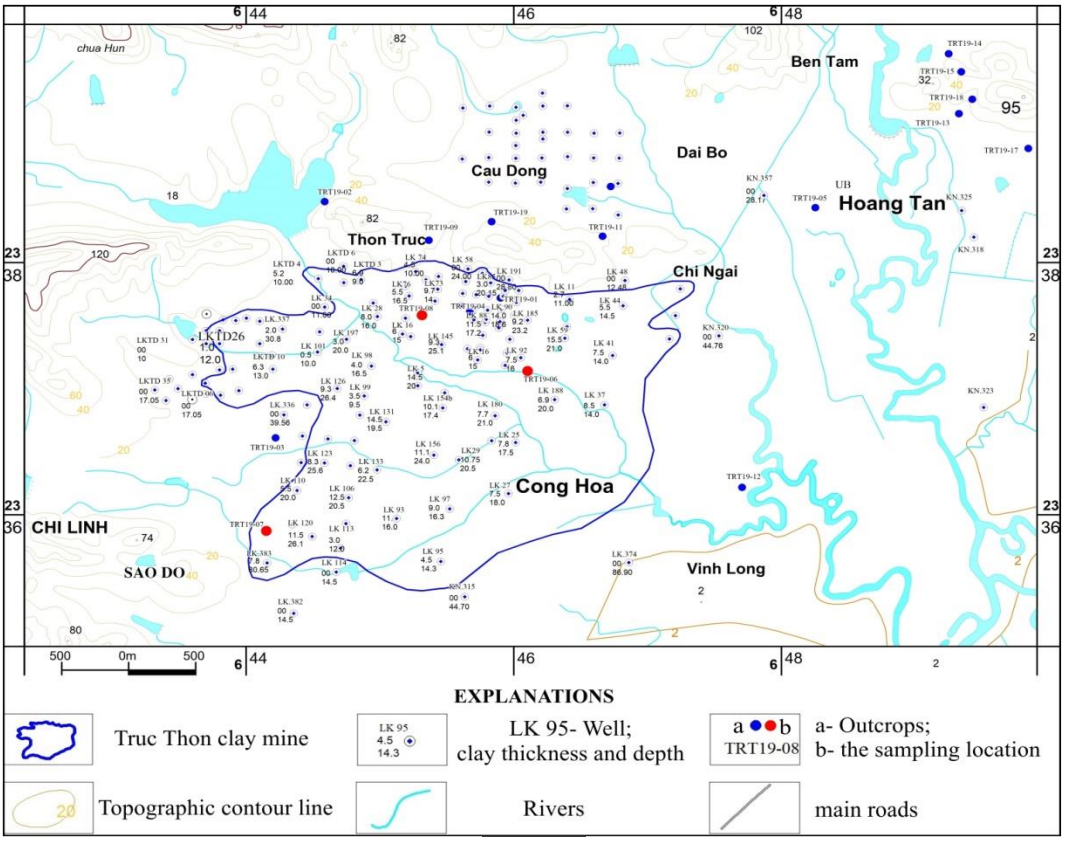

Figure 2. Sketch of the TTC mine distributionin the Hai Duong province (General Administration of the Land of Vietnam, 2005)

Interpretation of provenance is based on rare and trace elements. The geochemical proxies are calculated such as Th/Co vs. La/Sc, Cr/V vs. Y/Ni, La-Th-Sc, V-Ni-Th*10 ratio, Th/Sc vs. Eu/Eu*, Eu/Eu* vs. (Gd/Yb)N, Th/Sc vs. Zr/Sc. Geochemical proxies were used to interpret the provenance based on the works (e.g., Hiscott, 1984; Bhatia and Crook, 1986; McLennan et al., 1990; McLennan et al., 1993; Garcia et al., 1994; Cullers, 2002; Cullers and Podkovyrov, 2002; Bracciali et al., 2007). Besides, mineralogy and investigation of regional geology also play crucial roles.

4. Results

4.1. The distribution of TTC

The TTC mine belongs to Pha Lai-Dong Trieu Block, in KeBao-Dong Trieu structural Zone of the Northeast Coal Basin. The distribution area of the ceramic clay body is approximately 6.36 km^2 (Fig. 2). The mine is

in a pan-shaped terrain surrounded by low hills in the north, west, and south and extends to the east. The surface of the quarry is generally inclined gently from the north to the south with an altitude ranging from 15 m to 1.5 m.

The roof of the clay body lies at the depth below the overburden ca. 1.2-16.9m, while its floor surface ranges from 4m to 26.2m and curves along the topographic surface. The clay thickness ranges from 0.3 to 19.5m. It has a lenticular geometry with 2 types of clays, including white and grey-white clay above the patchy clay layer (Fig. 3). These develop continuously from the brown-yellow silty clay and clayey silt and are covered with sand and gravel above the surface, eroded. Analysis of good succession in the north and west shows clearly that the interfinger structure is intercalation of clay and sand.

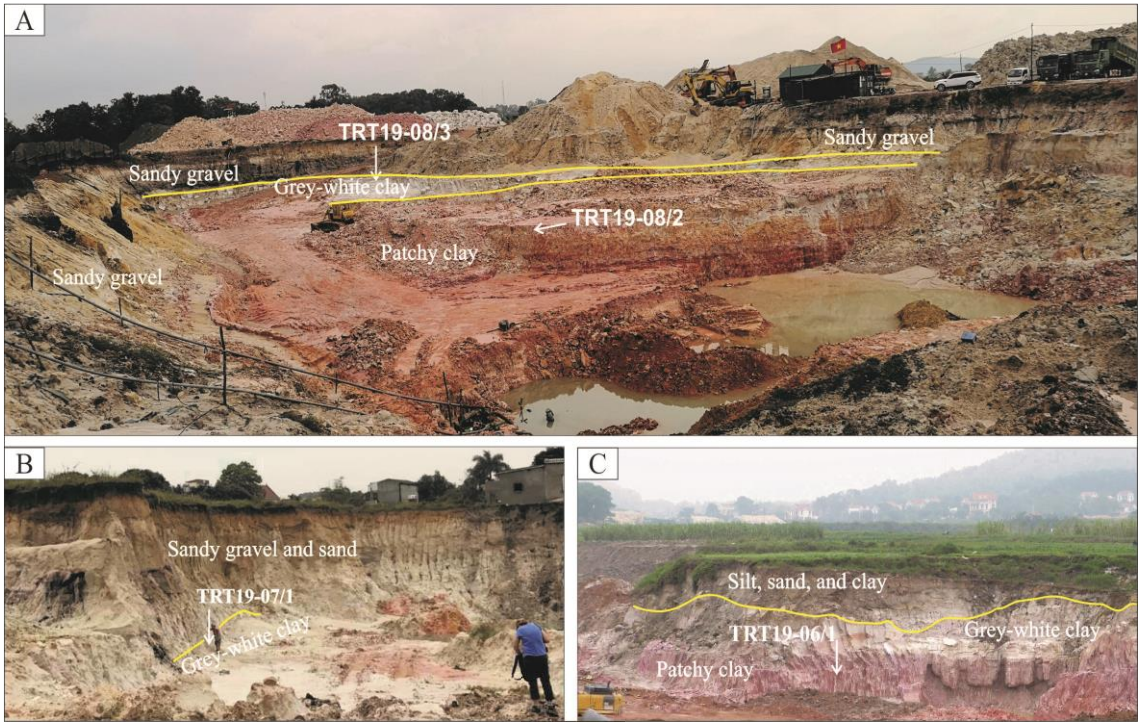

Figure3. General views of the exposures and position of samples: A-TRT19-08; B-TRT19-07 and C-TRT19-06 (SeeFigs.1, 2 for their locations)

The rocks of the Hon Gai Formation (T_3n-r*hg*) are exposed in the surrounding of the quarry, forming low mountainous hill terrain and basement. Within the trough comprise the Quaternary sediments of Vinh Phuc (Q_1^3*vp*), Hai Hung (Q_2^{1-2}*hh*), Thai Binh (Q_2^3*tb*) Formations (Fig. 1). These create quite a flat lowland terrain that tends to tilt to the south. The clay member concentrates in the Vinh Phuc Formation on the geological map (at a scale of 1:200,000) (Q_1^3*vp*) (Ky, 1999). In this study, a late Pleistocene age will be used for the TTC.

4.2. Bulk mineralogy and clay mineralogy

The TTC bulk mineralogy represents two assemblages: detritus minerals and clay minerals (Table 1; Fig. 4). The detritus consists of quartz (ca. 52-84%), feldspars (ca. 2-7%), rutile (ca. 0-1%), and hematite (ca. 0-1%). Clay minerals range from ca. 14-43% and include kaolinite, illite, pyrophyllite, chlorite, montmorillonite, and mixed-layer mineral (IS).

Table 1. Bulk minerals of the TTC. Abbreviations: Kao-Kaolinite, Ill-illite, Chl-Chlorite, Mnt-montmorillonite, Prl-Pyrophyllite; IS-mixed-layer

	Quartz	Feldspar	Rutile	Hematite	Kao	Ill	Mnt	IS	Chl	Prl
TRT19-06/1	57	7	1	1	17	9		4		4
TRT19-07/1	52	5			22	11	1		3	6
TRT19-08/2	73	2	1		15	6	<1			3
TRT19-08/3	60	3			18	10		3	1	5
TRT19-10/1	84	2	<1		5	7			1	1

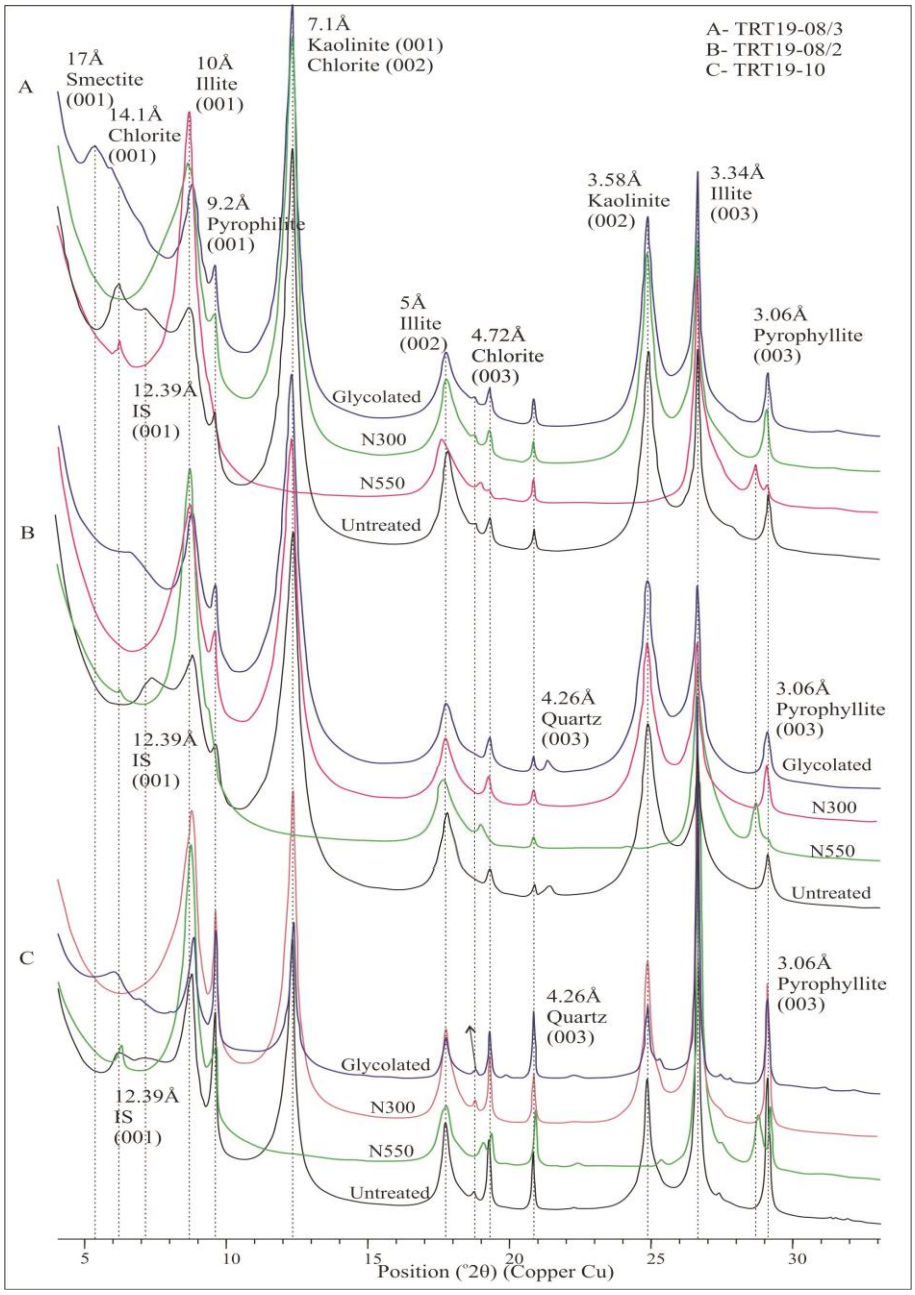

Figure 4. XRD patterns of clay fraction samples for the TTC

The TTC clay minerals include kaolinite, illite, chlorite, montmorillonite, vermiculite, and mixed-layer minerals such as illite-montmorillonite and illite-vermiculite (Tab. 2; Fig. 4). Mixed-layer clay minerals are identified by slight enlargement of the glycolate peak of smectite at 17 Å. Illite and mixed-layer minerals predominate (ca. 46-68%), and kaolinite is largely flocculated (ca. 25-51%) in the samples. A trace amount of minerals appears, such as zeolite, halloysite, which are not clearly displayed on the XRD patterns. Illite is commonly found in simultaneous alteration into both vermiculite and montmorillonite.

Table 2. Clay minerals of the TTC. Abbreviations: Kao - Kaolinite, Ill - illite, Chl - Chlorite, Mnt - montmorillonite, Vrm - Vermiculite

No.	Samples	Minerals and percentage (~%)						
		Kao	Ill	Chl	Mnt	Vrm	Mixed-layer (IS)	Others
1	TRT 19-08/2	51	24	1	-	-	24 (Illite-Montmorillonite, Illite- Vermiculite)	Pyrophyllite, zeolite, Halloysite
2	TRT19-08/3	31	17	2	3	3	44 (Illite-Montmorillonite)	Pyrophyllite, zeolite, Halloysite
3	TRT 19-10/1	25	22	5	-	2	46 (Illite-Vermiculite)	Pyrophyllite, zeolite, Halloysite

4.3. Bulk-rock geochemistry

4.3.1. Major elements

The concentration of major elements is based on estimation from 69 samples. The average, maximum, and minimum values for the major elements are presented in Table 3. The values of Upper Continental Crust (UCC) and Post Archaean Australian Shale (PAAS) are used in this study for comparison with the TTC samples.

Table 3. Major elemental concentrations (units: wt.%). STD denotes standard deviation values; CV is the coefficient of variation

	SiO_2	Al_2O_3	Fe_2O_3	MgO	CaO	Na_2O	K_2O	TiO_2	P_2O_5	MnO	Cr_2O_3	NiO	SO_3	LOI
Min	54.04	9.81	0.46	0.12	0.01	0.02	0.15	0.46	0.03	0.01	0.01	0.01	0.00	2.81
Max	84.00	28.38	7.53	0.99	0.85	1.23	2.39	1.60	0.34	0.04	0.02	0.01	0.24	9.89
Average	**65.56**	**21.05**	**2.27**	**0.32**	**0.27**	**0.36**	**1.26**	**0.81**	**0.17**	**0.02**	**0.01**	**0.01**	**0.06**	**6.18**
STD	6.84	4.35	1.62	0.16	0.26	0.27	0.57	0.23	0.09	0.01	0.01	0.00	0.05	1.44
CV	0.10	0.21	0.71	0.49	0.98	0.75	0.45	0.28	0.56	0.59	0.33	0.00	0.78	0.23
UCC	66.55	15.39	5.04	2.48	3.59	3.27	2.80	0.64	0.15	0.10	-	-	-	-
PAAS	62.80	18.90	7.23	2.20	1.30	1.20	3.70	1.00	0.16	0.11	-	-	-	-

The TTC geochemistry is heterogeneous, depending upon the depth as well as position of samples (Appendices 1, 2). Al_2O_3 is of high value (averages ca. 21.05%), while oxides such as CaO, MgO, TiO_2, P_2O_5, and MnO, are present only in low or trace amounts and relatively constant in the studied samples. Fe_2O_3 has a wide range ca. 0.46-7.53; however, the average value of the entire clay body (2.27) is still much lower than the UCC and PAAS. SiO_2 is associated with negative correlations, especially has strongly negative correlation with Al_2O_3 and LOI (Table 4). Al_2O_3 has just weak positive correlations with MgO and K_2O, while it is of a strongly positive correlation with LOI.

Geochemical proxies were used to interpret the paleoclimatic condition based on work by

Iqbal et al., 2019; Nesbitt and Young, 1982; Basu, 1976; Gromet et al., 1984; Nesbitt et al., 1996; Rudnick and Gao, 2003.

The values of Al_2O_3, CaO^*+NaO_2 and K_2O were used to for the A-CN-K plot (Nesbitt and Young, 1984; Bahlburg and Dobrzinski, 2011; Fig. 9C). The studied samples display a cluster near the A vertex close to the A-K side, clustered at A vertex corresponding to kaolinite-illite position (Fig. 9C).

Table 4. Correlation coefficient of the TTC major elements

	SiO_2	Al_2O_3	Fe_2O_3	MgO	CaO	Na_2O	K_2O	TiO_2	LOI
SiO_2	1								
Al_2O_3	**-0.92**	1							
Fe_2O_3	-0.38	0.05	1						
MgO	-0.48	0.27	**0.56**	1					
CaO	-0.03	0.22	-0.31	**-0.53**	1				
Na_2O	-0.15	0.06	0.03	0.03	-0.11	1			
K_2O	-0.08	0.24	-0.30	-0.32	**0.57**	-0.05	1		
TiO_2	-0.31	0.15	0.36	**0.60**	**-0.78**	0.17	-0.38	1	
LOI	**-0.86**	**0.88**	0.02	0.25	0.09	0.23	0.17	0.28	1

4.3.2. Rare and trace elements

Four samples were tested for Rare Earth Elements (REE) and trace elements from the TTC (Appendix 1). The average total REE content in the TTC is 215.28 ppm showing high enrichment relative to PAAS (184.77 ppm; Taylor and McLennan, 1985). The average Light Rare Earth Elements (LREE) is 197.40, and Heavy Rare Earth Elements (HREE) is 17.87, pointing to enrichment relative to PAAS. The average LREE/HREE ratio in the TTC (11.42) is enriched relative to PAAS (9.49; Taylor and McLennan, 1985). The REE in the entire TTC is generally enriched. However, these are spatially uneven for HREE, as shown in the REE depletion compared to UCC and PAAS (TRT19-06/1 and TRT19-07/1). The chondrite-normalized REE patterns for the studied samples are shown in Fig. 5. The patterns are variably enriched in LREE, and HREE patterns are flattened for TRT19-08/2 and TRT19-08/3 and fluctuated for TRT19-06/1 and TRT19-07/1. The average TTC anomaly is approximately 0.64, representing the Eu negative anomaly (Eu/Eu*).

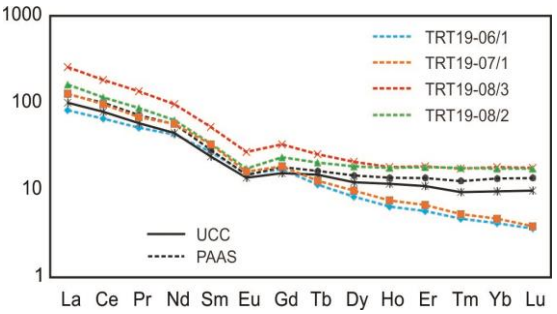

Figure 5. Chondrite-normalized rare earth element patterns of the studied samples (chondrite values from Boynton, 1985). UCC and PAAS values are plotted for comparison; UCC values are from Rudnick and Gao (2003); PAAS values are from Taylor and McLennan (1985)

Some parameters are calculated and established the plots to interpret provenance for the TTC. Th/Co ratios are high and fluctuating ca. 2.57-6.88 (mean: 4.64). La/Sc ratios are high and ranging ca. 2.15-5.25 (mean: 3.85) (Appendix I). Cr/V ratios are generally high and ranging ca. 0.79-2.13 (mean: 1.44). Y/Ni ratios are relatively high and fluctuating ca. 0.53-33.64 (mean: 10.14). Th/Sc ratios are relatively high and ranging ca. 1.13-1.72 (mean: 1.41). Zr/Sc ratios are variable with values ca. 0.2-37.74 (mean: 13.37). For sedimentology, Th/Sc vs. Zr/Sc

plot has an important sense for identifying sediment recycling and sorting processes (McLennan et al., 1993). The TTC samples align along the recycling line (Fig. 8A).

5. Discussions

5.1. Probable parent rocks

There have been many methods to interpret the source area of sedimentary materials (Ingersoll and Suczek, 1979; Dickinson and Valloni, 1980; Taylor and McLennan, 1985; Pettijohn et al. 1987; Cullers, 2002; Akarish and El-Gohary, 2008; Czarniecka et al., 2020). For the TTC, we used geochemical data, which is combined with field data and lithology to infer its provenance.

Trace element analysis suggests that the TTC samples were derived from silicic source rocks (Fig. 7A-E) (Hiscott, 1984; Bhatia and Crook, 1986; Cullers, 2002; Cullers and Podkovyrov, 2002; Bracciali et al., 2007). For TRT19-08/2 and TRT19-08/3, the chondrite-normalized REE patterns show that the LREE line is variably enriched, while HREE lines are flattened (Figs. 5, 6). This is expressed by the (La/Sm)N ratio, which has an average value of 4.82 (ca. 4.76-4.87), and the (Gd/Yb)N ratio with an average value of 1.59 (ca. 1.35-1.82). Moreover, the (La/Yb)N ratio demonstrates a total REE fractionation with a respective average of 11.61. TRT19-06/1 and TRT19-07/1 represent slight depletion of LREE and HREE compared with PAAS (Figs. 5, 6). However, together with the Eu anomalies, these results fit felsic source rock compositions (Taylor and McLennan, 1985; Cullers, 2002).

On the diagram of Eu/Eu* versus (Gd/Yb)N (Fig. 7F), the TRT19-08/2 and TRT19-08/3 samples plot within the post-Archean field, allowing for an interpretation that the deposits are linked to a post-Archean felsic protolith (Taylor and McLennan, 1985; McLennan et al., 1990). This fits the regional geological setting of northeast Vietnam (see Fig. 1), where the oldest formation is built by the Middle Cambrian rocks (Tri and Khuc, 2009; Tri et al., 2020). In comparison, TRT19-06/1 and TRT19-07/1 are of high values of (Gd/Yb)N (4.16 and 3.99) and plot towards an Archean felsic protolith (Fig. 7F). In the north of Vietnam, the Archean formation is only located in the northwestern zone, which the Red River Fault Zone separates (see Fig. 1, Tri and Khuc, 2009; Tri et al., 2020). This leads to difficulty infer exactly the sedimentary material source in the TTC clay during the Quaternary geological setting, and even the Tertiary period, in the northeast region. In this case, TRT19-06/1 and TRT19-07/1 show sedimentary material related to the Archean felsic protolith, which was further involved in multiple sedimentary recycling. We may assume the exhumated Archean crystalline basement or sedimentary sequence containing a redeposited Archean component (1) could have existed only for a short-time period, (2) had a relatively small range, and/or (3) due to complete erosion, does not occur in the modern geology of the north-eastern zone. However, more data points are needed for detailed studies in the future, from both the TTC and units from its surrounding.

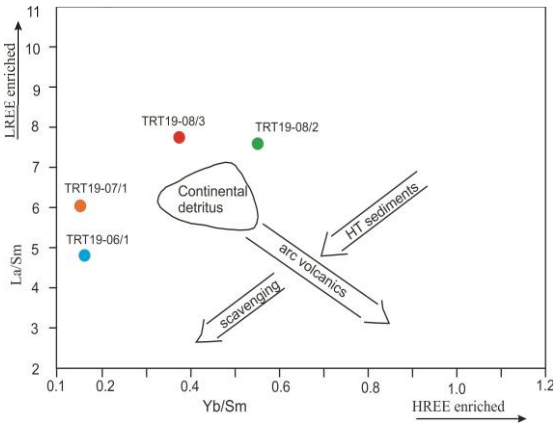

Figure 6. La/Sm versus Yb/Sm (Plank and Langmuir, 1998) is plotted for comparison between LREE - light rare earth elements and HREE- heavy rare earth element

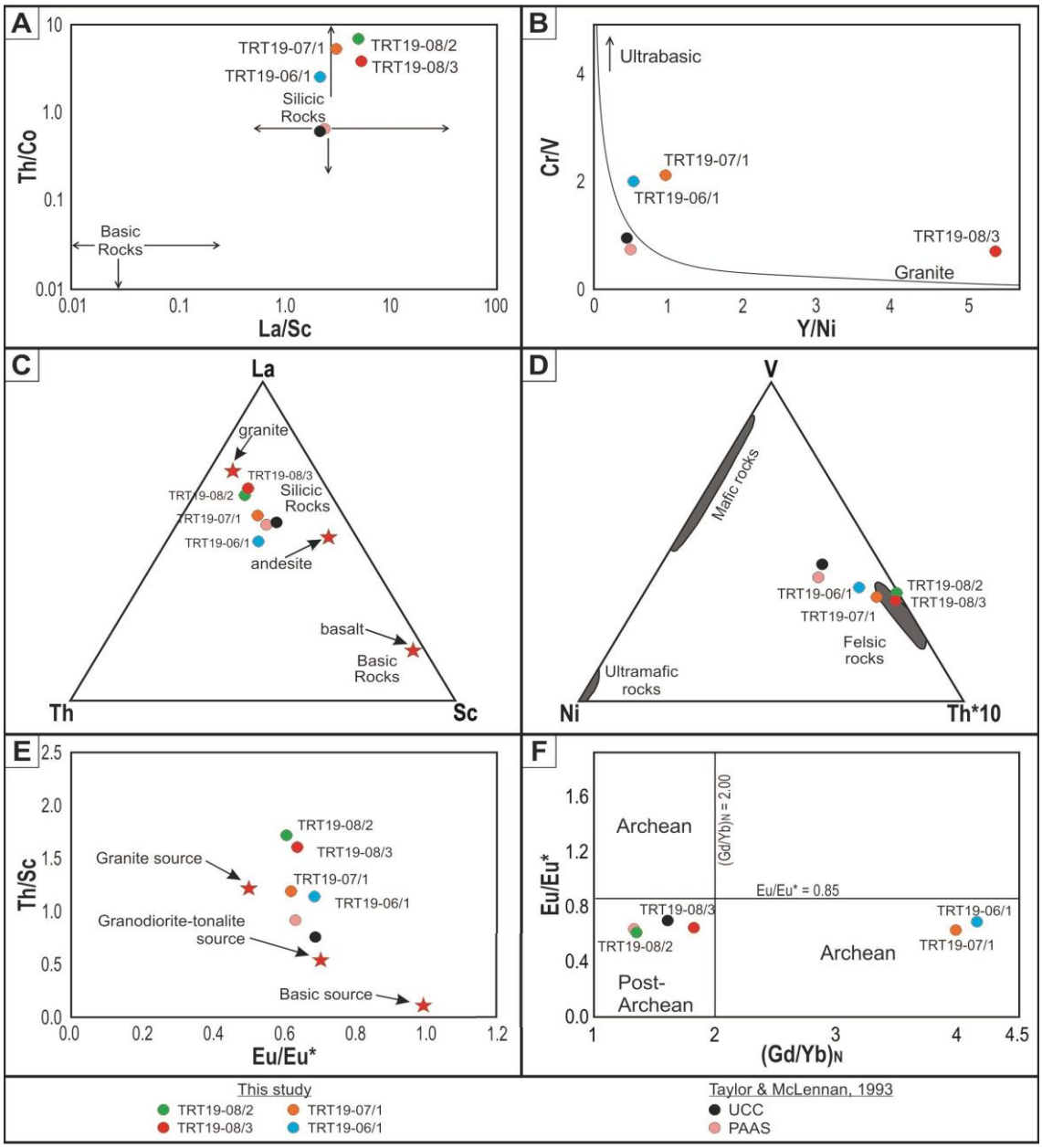

Figure 7. Selected trace elements and trace element ratios are useful for characterizing potential source rocks. (A) Th/Co vs. La/Sc diagram (Cullers, 2002) showing a silicic composition of source rocks for the studied deposits. (B) Cr/V vs. Y/Ni diagram (Hiscott, 1984) showing studied samples plotted between the granitic and UCC composition. (C) La-Th-Sc ternary diagram (Bhatia and Crook, 1986; Cullers, 2002) displaying the silicic composition of source rocks. Composition of basalt, andesite, and granite plotted for comparison. (D) The felsic source rocks composition is based on the V-Ni-Th*10 ratios (Bracciali et al., 2007). (E) Th/Sc vs. Eu/Eu* diagram (Cullers and Podkovyrov, 2002) linking potential sources to silicic rocks, mostly ranging between the granodiorite-tonalitic and granitic composition. (F) Eu/Eu* vs. (Gd/Yb)N diagram (McLennan et al., 1990) showing post-Archean felsic protolith as a proto source for the studied deposits

The geochemistry of the analyzed samples suggests that these deposits have chemical maturity and were probably reworked from older sedimentary rock sources. The recycling may be seen in the bulk rock trace element geochemistry. The Th/Sc vs. Zr/Sc ratio diagram (McLennan et al., 1993) consists of two trends (Fig. 8A). The first trend represents a compositional variation that correlates with a direct influx from primary sources. In contrast, the second one is related to sedimentary processes affecting the composition of the deposits. The Th/Sc value of studied samples (TRT19-08/3 and TRT19-08/2) range ca. 1.61-1.72, respectively, while Zr/Sc ratio expresses a relatively rise from 14.85 to 37.74 along the sedimentary recycling line. The Zr is an indicator of sediment recycling (McLennan et al., 1993) because it commonly concentrates on heavy minerals, particularly zircon, enriched in the sedimentation process. They are scattered in the $15*Al_2O_3$-Zr-$300*TiO_2$ plot (Fig. 8B, Garcia, et al., 1994), do not vary substantially with source composition, and the data seem to be less significant for the interpretation of the TTC provenance. For TRT19-06/1 and TRT19-07/1, they are of high values of Th/Sc (1.13 and 1.18, respectively) and low value of Zr/Sc ratios (0.7 and 0.2, respectively) (Fig. 8A). It clearly represents a source of sedimentary materials related to the Al-rich shales (Fig. 8B). These are suitable for the mineral composition of the studied samples. In the A-CN-K plot, the linear cluster of samples is distributed between A vertex and illite position along the A-K side (Fig. 9C). This is interpreted as a recycled origin of the sediments (Iqbal et al., 2019).

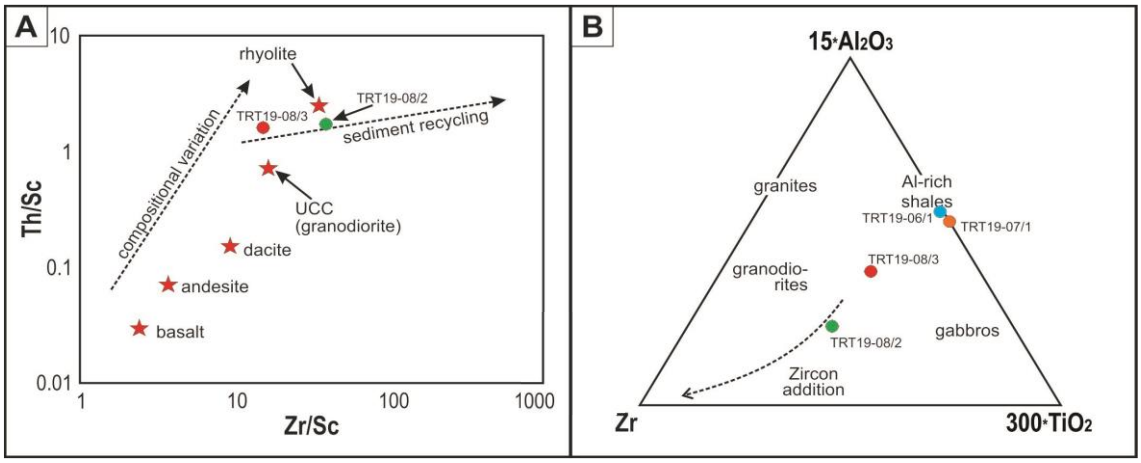

Figure 8. (A) Th/Sc versus Zr/Sc diagram (McLennan et al., 1993) showing data points for the studied deposits. Explanation in the text. (B) Diagram of $15*Al_2O_3$-Zr-$300*TiO_2$ ratio (Garcia et al., 1994) displaying barely accumulated the studied samples along the zircon addition arrow

Although many samples are tested for REE content, the results represent sedimentary geochemistry suitable to regional lithostratigraphic formations. A more accurate investigation of provenance is still based on the field data. The Triassic sedimentary formation of Hon Gai forms the basement of the study area (Fig. 1). Investigating the sedimentary rocks of Hon Gai Formation, it could easily find thick beds of multi-mineral conglomerates, sandstones, and quartz sandstones (TRT19-02, TRT19-09, TRT19-11, TRT19-20, TRT19-21, see Fig. 1) which are rich in quartz with angular to a very rounded shape. The multiple sedimentations may have created the Truc Thon upper

member rich in quartz and having perfect roundness. In the above-mentioned strata, there are layers and lenses of siltstones and siltyclaystones with grey, white, greenish grey, flesh pink color, and patchy weathered sedimentary rocks. Besides, the TTC clay contains a high amount of quartz, feldspar, and pyrophyllite (Table 1). Pyrophyllite commonly appears in metamorphic rocks and the diagenesis stage of sedimentary rocks. Therefore, it indicates the inheritance of materials from previous sedimentary rocks, which experienced diagenesis processes.

On these bases, the source area of sedimentary materials was probably located in the north of the study area.

5.2. Signature of paleoclimate

There are many methods to reconstruct paleoclimatic conditions; however, each geological formation must have suitable indicators. The TTC contains inferior content of organic matter, lacks both indicative fauna and flora fossils. Therefore, the geochemical proxies become effective tools to differ paleoclimate conditions during sedimentation.

The CIA is a more sensitive indicator for prevailing paleoclimate (Nesbitt and Young, 1984; Iqbal et al., 2019). The TTC is of CIA value ca. 80.6-98.0 (average 90.4). The CPA values represent a range from 89.8 to 99.8 (average 97.1). In general, the CIA and CPA values show similar trends. The PIA is ca. 86.7-99.2 (average 94.7). It indicates a very high intensity of chemical weathering (Bahlburg and Dobrzinski, 2011). Values of the CIW (Harnois, 1988) confirm the high degree of chemical weathering in a range of ca. 87.9-99.3 (average 95). The PIA, which shows progressive weathering of feldspars to clay minerals, presents very high values (ca. 86.7-99.2). It means that intensive destruction of feldspar took place during source rocks weathering, transport, deposition, and/or diagenetic processes. These geochemical proxies may reflect the hot - humid tropical near tropical paleoclimate (Iqbal et al., 2019).

The overall Al_2O_3 content of the TTC is very high (ca. 9.81-28.38%, average 21.05%), almost all the samples are over 15% (Fig. 9A). Na_2O and K_2O contents are relatively constant in samples, but the remark is that K_2O/Na_2O is very changeable (ca. 0.14-47.67) (Fig. 9B). This may be related to local mobility and the exchange of positive ions. K_2O/Al_2O_3 is relatively constant ca. 0.01-0.10. SiO_2/Al_2O_3 ratios range ca 1.90-8.56. The $CIA_{(molar)}$ is ca. 4.1-49.6 (mean 13.8) (Goldberg and Humayun, 2010). These features with high CIA values support overall tropical conditions. The Al_2O_3 vs. CIA plot of these intervals indicates tropical climate that is also fixed by the K_2O/Na_2O vs. CIA plot (Fig. 9A, B).

The A-CN-K plot (Nesbitt and Young, 1984; Bahlburg and Dobrzinski, 2011; Iqbal et al., 2019) explains the link between weathering trends and mineralogical compositions (Basu, 1976). A positive correlation of TiO_2 with Al_2O_3 in the studied samples suggests that chemical weathering in the source area was an important process controlling their mineralogy (Tab.3). The A-CN-K diagram and the CIA values link the studied samples to strong weathering and suggest the weathering intensity condition (Fig. 9C). It is worth noting that the-CN-K diagram samples plot along the weathering trend line for the UCC and do not show any inclination towards the K-apex. The samples occupy positions in the high illite-kaolinite zone (Fig. 9C). This lets us suspect that the studied deposits did not experience potassium remobilization, e.g., due to metasomatism, metamorphism, or diageneticillitization. The studied deposits are composed of particles recycled from older sedimentary strata originally related to silicic rocks, granite-granodiorite-like composition based on trace element geochemistry. The ICV (Cox et al., 1995) counted in this study confirms a lack of

a first cycle input (Fig. 10). This agrees with the obtained CIA values (Figs. 9A, B). The A-CN-K plot shows a cluster of these samples in the kaolinite zone, confirming their supreme mature stage of chemical alteration (Fig. 9C). This strongly supports recycling under a hot/warm and humid paleoclimate (Iqbal et al., 2019).

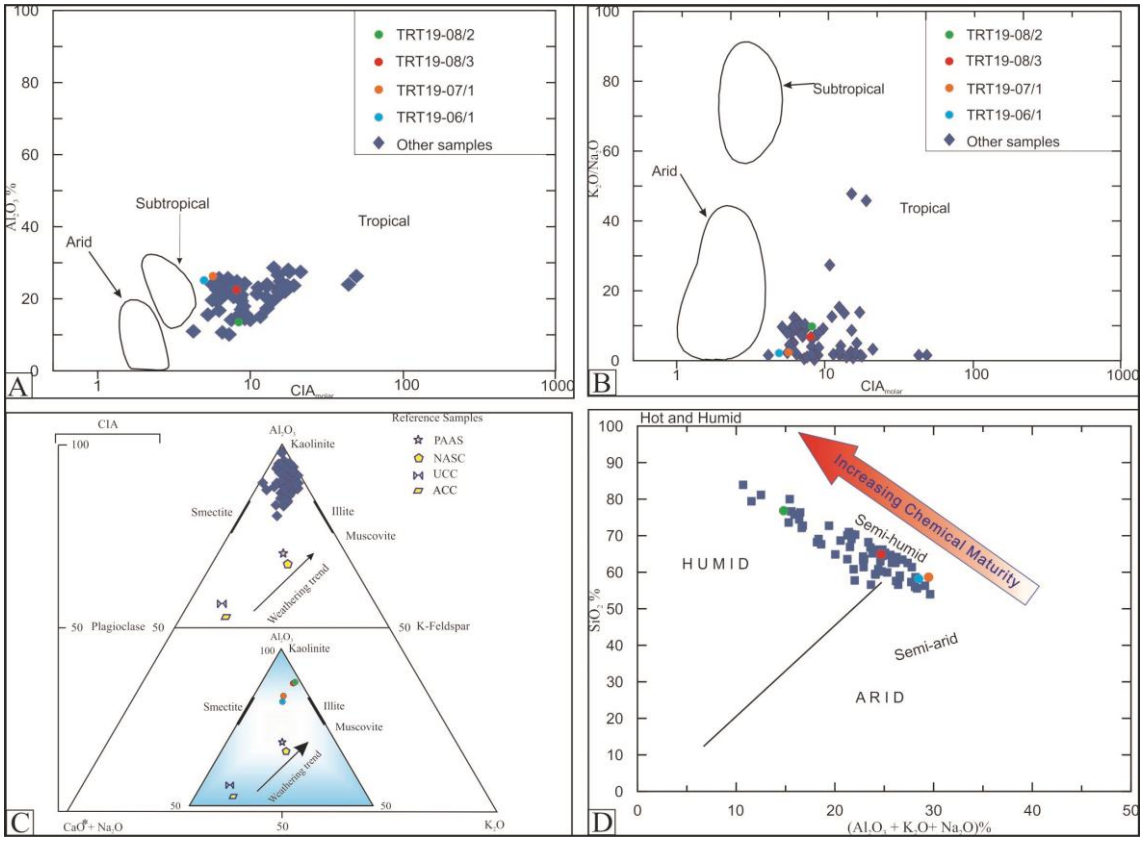

Figure 9. (A) Al_2O_3 vs. Chemical Index of Alteration ($CIA_{(molar)}$) plot for the representative samples. (B) K_2O/Na_2O vs. $CIA_{(molar)}$ plot for representative samples. (C) Al_2O_3-CaO + Na_2O-K_2O (A-CN-K) plot for the representative samples, positions of reference minerals (muscovite, illite, smectite, and kaolinite) are indicated on the plot (Basu, 1976; Nesbitt et al., 1996). The reference samples include Post Archaean Australian Shale (PAAS), North American Shale Composite (NASC), Upper Continental Crust (UCC), and Average Continental Crust (ACC) (Gromet et al., 1984; Nesbitt et al., 1996; Rudnick and Gao, 2003). (D) Compositional maturity proxy plot for SiO_2% vs. (Al_2O_3+K_2O+Na_2O)% showing paleoclimatic conditions during the deposition

The chemical maturity proxy plot (SiO_2 vs. Al_2O_3+Na_2O+K_2O) represents a correlation between the increasing SiO_2 content and Al_2O_3+Na_2O+K_2O for the TTC (Fig. 9D) and indicates gradually increasing siliciclastic influx. It means increased chemical maturity. The samples plot drops from semi-humid to humid zones. Thus, samples represent a changeable trend from semi-humid paleoclimate to humid paleoclimate (Fig. 9D).

The clay mineralogy does not show a good indication for the climatic conditions of sediment formation because the mineral assemblage is very complex in the TTC. The minerals of quartz, feldspar, pyrophyllite indicate inheritance of sedimentary materials

from bedrocks of the source area. The presence of feldspar clearly indicates an origin of kaolinites and might be originated from a composition of the Hon Gai claystones and clayey siltstones. Certainly, kaolinite is present in high amounts, which usually displays the absolute chemical weathering of sedimentary materials in the condition of warm-hot and humid paleoclimate (Iqbal et al., 2019).

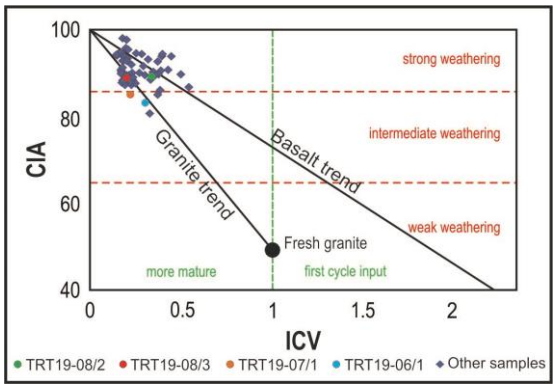

Figure 10. CIA versus ICV diagram (Lee, 2002; Potter et al., 2005) showing strong chemical weathering resulted in a lack of first cycle sediment input into the studied deposits

On these bases, source rocks for the studied deposits were located under tropical climate, and differences in semi-humidity to humidity can be observed. As the siliciclastic grains were recycled from older sedimentary units, the differences in humidity may point to changes in the hinterland composition in time.

6. Conclusions

The TTC data is rich, but it has been ignored scientific potential. This study provides a fuller worth for the TTC by analyzing provenance and paleoclimate based on mineralogy and geochemical proxies. The discrimination plots of Th/Co vs. La/Sc, Cr/V vs. Y/Ni, La-Th-Sc, V-Ni-Th*10, Th/Sc vs. Eu/Eu*, Eu/Eu* vs. (Gd/Yb)N and concentration of REE show quite complex in provenance, but it distinctly demonstrates a linkage to a post-Archean felsic protolith. Sedimentary materials are originally related to silicic rocks, rocks of granite–granodiorite–like composition. The high values of quartz, pyrophyllite, illite indicate inheritance of older sedimentary rocks. They are supported by the plots of Th/Sc vs. Zr/Sc, 15*Al_2O_3-Zr-300*TiO_2, and A-CN-K by sediment recycling. Combined with regional geological features, the Hon Gai Triassic rocks are proposed as a main source for the TTC.

The dominance of quartz and kaolinite indicates the highly mineralogical and chemical maturity of the TTC. The source area had undergone under conditions of extreme chemical weathering, proven by very high CIA values and geochemical proxies. This indicates a warm/hot and semi-humid/humid tropical climate.

Acknowledgements

This paper is supported by the project code VAST05.01/19-20. We express our gratitude to Dr. Bui Van Thom, Assoc. Prof. Doan Dinh Lam, and MSc. Nguyen Minh Quang for their consultations and help in the field work.

References

Akarish A.I.M., El-Gohary A.M., 2008. Petrography and geochemistry of lower Paleozoic sandstones, East Sinai, Egypt: Implications for provenance and tectonic setting. Journal of African Earth Sciences, 52, 43-54.

Bahlburg H., Dobrzinski N., 2011. A review of the Chemical Index of Alteration (CIA) and its application to the study of Neoproterozoic glacial deposits and climate transitions. Geol. Soc. Lon. Memoirs, 36(1), 81-92.

Basu A., 1976. Petrology of Holocene fluvial sand derived from plutonic source rocks: Implication to paleoclimatic interpretation. J. Sed. Petrol., 46, 694-709.

Bhatia M.R., Crook K.A.W., 1986. Trace element characteristics of greywackes and tectonic setting discrimination of sedimentary basins. Contributions to Mineralogy and Petrology, 92, 181-193.

Böhme M., Prieto J., Schneider S., Hung N.V., Quang D.D., Tran D.N., 2011. The Cenozoic on-shore basins of Northern Vietnam: Biostratigraphy, vertebrate and invertebrate faunas. Journal of Asian Earth Sciences, 40, 672-687.

Boynton W.V., 1985. Cosmochemistry of the rare earth elements: meteorite studies. In Henderson P. (ed.): Rare Earth Element Geochemistry. Elsevier, Amsterdam, 63-114.

Bracciali L., Marroni M., Pandolfi L., Rocchi S., 2007. Geochemistry and petrography of Western Tethys Cretaceous sedimentary covers (Corsica and Northern Apennines): from source areas to configuration of margins. In Arribas J., Critelli S., Johnsson M.J. (eds.): Sedimentary Provenance and Petrogenesis: Perspectives from Petrography and Geochemistry. Geological Society of America Special Paper, 420, 73-93.

Cox R., Low D.R., Cullers R.L., 1995.The influence of sediment recycling and basement composition on evolution of mudrock chemistry in the southwestern United States. Geochimica and Cosmochimica Acta, 59, 2919-2940.

Cullers R.L., 2002: Implications of elemental concentrations for provenance, redox conditions, and metamorphic studies of shales and limestones near Pueblo. CO. USA. Chemical Geology, 191, 305-327.

Cullers R.L., Podkovyrov V.N., 2002. The source and origin of terrigenous sedimentary rocks in the Mesoproterozoic Ui group, southeastern Russia. Precambrian Research, 117, 157-183.

Czarniecka U., Haile B.G., Braathen A., Krajewski K.P., Kristoffersen M., Jokubauskas P., 2020. Petrography, bulk-rock geochemistry, detrital zircon U-Pb geochronology and Hf isotope analysis for constraining provenance: An example from Middle Triassic deposits (Bravaisberget Formation), Sørkappøya. Svalbard. Norwegian Journal of Geology, 100, 202017.

Dickinson W.R., Valloni R., 1980. Plate settings and provenance of sands in modern ocean basins. Geology, 8, 82-86.

Diet D. (ed.), 1975. Report on Establishing of the geological sketch of Dong Trieu area, Quang Ninh province, at 1:50,000 scale. General Department of Geology of Vietnam. Hanoi (in Vietnamese).

Fedo C.M., Nesbitt H.W., Young G.M., 1995. Unravelling the effects of potassium metasomatism in sedimentary rocks and paleosols, with implications for paleoweathering conditions andprovenance. Geology, 23, 921-924.

Garcia D., Fonteilles M., Moutte J., 1994. Sedimentary fractionations between Al, Ti, and Zr and the genesis of strongly peraluminous granites. Journal of Geology, 102, 411-422.

Garver J.I., Royce P.R., Smick T.A., 1996. Chromium and nickel in shale of the Taconic foreland: a case study for the provenance of fine-gained sediments with an ultramafic source. Journal of Sedimentary Research, 66, 100-106.

Goldberg K., Humayun M., 2010. The applicability of the Chemical Index of Alteration as a paleoclimatic indicator: An example from the Permian of the Paraná Basin. Brazil. Palaeogeography. Palaeoclimatology. Palaeoecology, 293, 175-183.

Gromet L.P., Haskin L.A., Korotev R.L., Dymek R.F., 1984. The “North American shale composite”: its compilation, major and trace element characteristics. Geochim. Cosmochim. Acta, 48(12), 2469-2482.

Harnois L., 1988. The CIW index; a new chemical index of weathering. Sedimentary Geology, 55, 319-322.

Hiscott R.N., 1984. Ophiolitic source rocks for Taconic-age flysch: trace element evidence. Geological Society of America Bulletin, 95, 1261-1267.

Hofer G., M. Wagreich, S. Neuhuber, 2013. Geochemistry of fine-grained sediments of the upper Cretaceous to Paleogene Gosau Group (Austria, Slovakia): Implications for paleoenvironmental and provenance studies. Geoscience Frontiers, 4, 449-468.

Hofmann P., Ricken W., Schwark L., Leythaeuser D., 2001. Geochemical signature and related climatic-oceanographic processes for early Albian black shales: site 417D. North Atlantic Ocean. Cretaceous Research, 22, 243-257.

Huyen N.X. (ed.), 1996. Report on investigating the quality and reserves of clay mineral in the Red River Plain: Orienting exploitation and rational use of raw materials. Institute of Geological Sciences. Vietnam Academy of Science and Technology. Hanoi (in Vietnamese).

Ingersoll R.V., Suczek C.A., 1979. Petrology and provenance of Neogene sand from Niconbar and Bengal Fans, DSDP sites 211 and 218. Journal of Sedimentary Petrology, 49, 1217-1228.

Iqbal S., Wagreich M., Jan I., Kuerschner W. M., Gier S., Bibi M., 2019. Hot-house climate during the Triassic/Jurassic transition: The evidence of climate change from the southern hemisphere (Salt Range,

Pakistan). Global and Planetary Change, 172, 15-32.

Ky H.N. (ed.), 1999. Geology and mineral resources of the Hai Phong Map sheet, with the Geological Map of the Ha Long Sheet at 1:200,000 scale. General Department of Geology and Minerals of Vietnam. Hanoi (in Vietnamese).

Lan T.T., Duong N.A., Anh P.L., Man T.T., 2019. Research on fabrication of non-calcined geopolymer ceramics from kaolin Tung Ba, Vi Xuyen, Ha Giang. Vietnam Journal of Earth Sciences, 41(4), 388-402.

Lee Y.I., 2002. Provenance derived from the geochemistry of late Paleozoic-early Mesozoic mudrocks of the Pyeongan Supergroup. Korea. Sedimentary Geology, 149, 219-235.

Long N.V. (ed.), 2006. Report on exploration of the refractory clay in the Truc Thon area, Cong Hoa commune, Chi Linh district, Hai Duong province. General Department of Geology of Vietnam. Hanoi (in Vietnamese).

Luc V.X. (ed.), 2017. Geological Map F-48-69-D (Pha Lai sheet), at 1:50,000 scale. General Department of Geology and Minerals of Vietnam. Hanoi (in Vietnamese).

Ly P.T., Thuy H.L.T., 2019. Spatial distribution of hot days in north central region, Vietnam in the period of 1980-2013. Vietnam Journal of Earth Sciences, 41(1), 36-45.

Madhavaraju J., González-León C.M., Lee Y.I., Armstrong-Altrin J.S., Reyes-Campero L.M., 2010.Geochemistry of the Mural Formation (Aptian-Albian) of the Bisbee Group, Northern Sonora. Mexico. Cretaceous Research, 31, 400-414.

Man T.T., Lan T.T., Duong N.A., Anh P.L., 2020. Assessment of the usability of Tam Bo bentonite (Di Linh - Lam Dong for peloid. Vietnam Journal of Earth Sciences, 42(4), 384-394.

McLennan S.M., Hemming S., McDaniel D.K., Hanson G.N., 1993. Geochemical approaches to sedimentation, provenance and tectonics. In Johnsson M.J., Basu A. (eds.): Processes Controlling the Composition of Clastic Sediments. Geological Society of America Special Paper, 284, 21-40.

McLennan S.M., Taylor S.R., McCulloch M.T., Maynard J.B., 1990. Geochemical and Nd-Sr isotopic composition of deep-sea turbidites-crustal evolution and plate tectonic associations. Geochimica et Cosmochimica Acta, 54, 2015-2050.

Miall A.D., 2006. The Geology of Fluvial Deposits. Springer-Verlag. Berlin, 589pp.

Nesbitt H.W., Young G.M., 1984. Prediction of some weathering trends of plutonic and volcanic rocks based upon thermodynamic and kinetic consideration. Geochimica et Cosmochimica Acta, 48, 1523-1534.

Nesbitt H.W., Young G.M., McLennan S.M., Keays R.R., 1996. Effects of chemical weathering and sorting on the petrogenesis of siliciclastic sediments, with implications for provenance studies. J. Geol., 104(5), 525-542.

Nesbitt H.W., Young G.W., 1982. Early Proterozoic climates and plate motions inferred from major element chemistry of lutites. Nature, 299, 715-717.

Pettijohn F.J., Potter P.E., Siever R., 1987. Sand and sandstones. 2nd ed. Springer-Verlag. New York, 61pp.

Plank T., Langmuir C.H., 1998. The chemical composition of subducting sediment and its consequences for the crust and mantle: Chemical Geology, 145, 325-394.

Potter P.E., Maynard J.B., Depetris P.J., 2005. Mud and mudstones. Springer Science and Business Media, 297pp.

Rahman M.J.J., Suzuki S., 2007. Composition of Neogene shales from the Surma Group, Bengal Basin, Bangladesh: implications for provenance and tectonic setting. Austrian Journal of Earth Sciences, 100, 54-64.

Roser B.P., Korsch R.J., 1988. Provenance signatures of sandstone-mudstone suites determined using discriminant function analysis of major-element data. Chemical Geology, 67, 119-139.

Rudnick R.L., Gao S., 2003.Composition of the continental crust. In Holland H.D., Turekian K.K. (eds.): Treatise on Geochemistry. Elsevier-Pregamon. Oxford-London, 3, 1-64.

Song A., Liu J., Liang S.-Q., Van Do T., Nguyen H.B., Deng W.-Y.-D., Jia L.-B., Del Rio C., Srivastava G., Feng Z., Zhou Z.-K., Huang J., Su T., 2021. Leaf fossils of Sabalites (Arecaceae) from the Oligocene of northern Vietnam and their paleoclimatic implications. Plant Diversity. https://doi.org/10.1016/j.pld.2021.08.003.

Taylor S.R., McLennan S.M., 1985. The continental crust: its composition and evolution. Blackwell Scientific Publications. Oxford, 312pp.

Tha H.V., Anna W., Cuong N.Q., Thom B.V., Lam D.D., Pha P.D., Huyen N.X., Tuan D.M., Ha V.V., Thanh N.T., Min N.T., Quang N.M., Chi G.T.K., 2019. Preliminary study results on lithofacies and depositional environment in the area of the clay

mine of the Truc Thon depression, NE Vietnam. Proceedings of The Third National Conference on Marine Geology. Publishing House for Science and Technology. Hanoi. Vietnam, 171-172.

Ti D.Q. (ed.), 1985. Geological report on meticulous exploration of the refractory clay mine in Truc Thon - Hai Hung. General Department of Geology of Vietnam. Hanoi (in Vietnamese).

Tri T.V., Khuc V. (eds), 2009. Geology and Natural Resources of Vietnam. Natural Science and Technics Publishing House. Hanoi, 589pp.

Tri Van Tran, Michel Faure, Vuong Van Nguyen, Hoang Huy Bui, Michael Bryl Wessel Fyhn, Tuan Quang Nguyen, Claude Lepvrier, Tonny B. Thomsen, Kenichiro Tani, Punya Charusiri, 2020. Neoproterozoic to Early Triassic tectono-stratigraphic evolution of Indochina and adjacent areas: A review with new data. Journal of Asian Earth Sciences, 191, 1-23.

Tuyet N.T., Thanh N.D., Tan P.V., 2019. Performance of seaclid/cordex-sea multi-model experiments in simulating temperature and rainfall in Vietnam. Vietnam Journal of Earth Sciences, 41(4), 374-387.

Wysocka A., Pha P.D., Durska E., Czarniecka U., Thang D.V., Filipek A., Cuong N.Q., Tuan D.M., Huyen N.X., Tha H.V., Staniszewski R.Ł., 2020. The Na Duong Basin (North Vietnam): a key for understanding Paleogene basin evolution in relation to the left-lateral Cao Bang-Tien Yen Fault. Journal of Asian Earth Sciences, 195, 1-20. Doi.org/10.1016/j.jseaes.2020.104350.

Zachos J., Pagani M., Sloan L., Thomas E., Billups K., 2001. Trends, rhythms and aberrations in global climate 65 Ma to Present. Science, 292, 686-693.

Appendix 1. Geochemical data of the TTC samples tested by the modern method; UCC and PASS values are for comparison

ICP-ES [wt. %]														
		SiO_2	Al_2O_3	Fe_2O_3	MgO	CaO	Na_2O	K_2O	TiO_2	P_2O_5	MnO	Cr_2O_3	LOI	Sum
	MDL	0.01	0.01	0.04	0.01	0.01	0.01	0.01	0.01	0.01	0.01	0.002	-5.1	0.01
No	Sample													
1	TRT19-08/2	76.6	13.45	1.95	0.22	0.04	0.13	1.23	1.01	0.03	<0.01	0.01	5.2	99.88
2	TRT19-08/3	64.65	22.41	0.88	0.32	0.07	0.3	1.99	1.02	0.05	<0.01	0.012	8.1	99.86
3	TRT19-06/1	57.96	24.86	2.4	0.45	0.22	1.23	2.39	0.96		<0.01	0.023	8.53	99.00
4	TRT19-07/1	58.34	26.14	0.81	0.42	0.18	1.11	2.24	1.16		<0.01	0.023	9.01	99.41
UCC (Rudnick and Gao, 2003)		66.55	15.39	5.04	2.48	3.59	3.27	2.80	0.64	0.15	0.10			100.00
PAAS (Taylor and McLennan, 1985)		62.80	18.90	7.23	2.20	1.30	1.20	3.70	1.00	0.16	0.11			98.60

ICP-MS [ppm]												
		Ba	Be	Co	Cs	Ga	Hf	Nb	Rb	Sc	Sn	Sr
	MDL	1	1	0.2	0.1	0.5	0.1	0.1	0.1	1	1	0.5
No	Sample											
1	TRT19-08/2	267	3	2.5	10.2	15.5	10.3	21.6	81.2	10	4	66.8
2	TRT19-08/3	448	3	6.3	15.6	28.8	5.9	20.4	119.9	15	5	114.7
3	TRT19-06/1	282		5.2		48.7			71.7	12		50.2
4	TRT19-07/1	354		2.9		64.7			82.2	13		71.3
UCC (Rudnick and Gao, 2003)		628.00		17.30	4.90	17.5	5.30	12.00	82.00	14.00	2.1	320.00
PAAS (Taylor and McLennan, 1985)		650.00		23.00	15.00	20	5.00	19.00	160.00	16.00		200.00

ICP-MS [ppm]												
		Ta	Th	U	V	W	Zr	Y	La	Ce	Pr	Nd	Sm
	MDL	0.1	0.2	0.1	8	0.5	0.1	0.1	0.1	0.1	0.02	0.3	0.05
No	Sample												
1	TRT19-08/2	1.6	17.2	4.1	90	3	377.4	37	49.6	92.9	10.45	37.5	6.55
2	TRT19-08/3	1.5	24.1	4.6	116	4.4	222.8	39.1	78.7	145	16.24	57.6	10.17
3	TRT19-06/1		13.4		89		8.3	12.0	25.4	52.6	6.21	25.6	5.27
4	TRT19-07/1		15.1		82		2.5	14.6	38.9	76.5	8.32	34.0	6.44
UCC (Rudnick and Gao, 2003)		0.90	10.50	2.70	97.00	1.9	193.00	21.00	31.0	63.0	7.1	27.0	4.70
PAAS (Taylor and McLennan, 1985)		1.50	14.60	3.10	150.00		210.00	27.00	38.2	79.6	8.8	33.9	5.55

ICP-MS [ppm]												
		Eu	Gd	Tb	Dy	Ho	Er	Tm	Yb	Lu	Mo	Cu
	MDL	0.02	0.05	0.01	0.05	0.02	0.03	0.01	0.05	0.01	0.1	0.1
No	Sample											
1	TRT19-08/2	1.27	6.03	0.97	5.92	1.27	3.81	0.58	3.61	0.56	0.2	2.2
2	TRT19-08/3	2	8.57	1.21	6.74	1.29	3.91	0.56	3.8	0.57	0.3	12.3
3	TRT19-06/1	1.11	4.40	0.55	2.68	0.46	1.20	0.15	0.85	0.11		
4	TRT19-07/1	1.17	4.79	0.60	3.10	0.54	1.40	0.17	0.97	0.12		
UCC (Rudnick and Gao, 2003)		1.00	4.00	0.70	3.90	0.83	2.30	0.30	2.00	0.31	1.1	28.00
PAAS (Taylor and McLennan, 1985)		1.08	4.66	0.77	4.68	0.99	2.85	0.41	2.82	0.43	1	50.00

ICP-MS [ppm]													
		Pb	Zn	Ni	As	Cd	Sb	Bi	Ag	Au	Hg	Tl	Se
	MDL	0.1	1	0.1	0.5	0.1	0.1	0.1	0.1	0.5	0.01	0.1	0.5
No	Sample												
1	TRT19-08/2	11.1	5	1.1	1.5	<0.1	1.3	0.3	<0.1	2.7	0.03	0.1	<0.5
2	TRT19-08/3	20.1	5	7.2	<0.5	<0.1	0.9	0.4	<0.1	1.9	0.19	0.2	<0.5
3	TRT19-06/1			22.5									
4	TRT19-07/1			15.1									
UCC (Rudnick and Gao, 2003)		17	67.00	47.00	4.80	0.09	0.4	0.16	53		0.05	0.9	0.09
PAAS (Taylor and McLennan, 1985)		20	85.00	55.00									

ICP-ES - Inductively Coupled Plasma - Emission Spectrometry; ICP-MS - Inductively Coupled Plasma - Mass Spectrometry; wt. % - Weight percent; ppm - Parts per million; MDL - Measurement detection limit; LOI - Lost on ignition ($^{\#}$ by weight difference after ignition at 1000°C)

Appendix 2. Geochemical data of the TTC samples tested by the XRF and collected samples; UCC and PASS values are for comparison

XRF [wt. %]														
		SiO_2	Al_2O_3	Fe_2O_3	MgO	CaO	Na_2O	K_2O	TiO_2	P_2O_5	MnO	Cr_2O_3	LOI	Sum
	MDL	0.01	0.01	0.01	0.01	0.01	0.01	0.01	0.01	0.01	0.01	0.01	#	
No	Samples													
1	TRT19-8/3a	64.19	23.4	0.99	0.45	0.08	0.33	1.99	1.16	0.04	0.01	0.019	7.03	99.694
2	TRT19-8/2a	72.82	17.72	1.67	0.39	0.05	0.2	1.44	1.12	0.03	0.01	0.013	4.56	100.028
3	TRT19-10	80.00	13.86	0.63	0.33	0.08	0.15	1.35	0.79	0.03	0.01	0.013	2.81	100.058
Samples (No4-65) are collected from Ti et al., 1985; Long 2006 (in reference)														
4	LKCD4/03	66.76	21.57	0.72	0.18	0.59	0.16	1.85	0.68	0.19	0.01		6.73	99.51
5	LKCD2/01	70.15	19.25	0.84	0.12	0.53	0.19	1.77	0.5	0.12			6.02	99.67
6	LKCD2/02	70.26	20.08	0.69	0.14	0.56	0.21	1.75	0.6	0.13			5.05	99.64
7	LKTD2/16	69.15	19.81	3.71	0.14	0.61	0.14	1.7	0.52	0.14			3.63	99.67
8	LKTD7/12	72.27	15.37	3.18	0.21	0.85	0.12	1.13	0.52	0.13	0.02		5.37	99.23
9	LKTD24/08	66.19	22.21	1.55	0.18	0.61	0.21	1.79	0.5	0.17	0.01		6.21	99.72
10	LKTD7/20	66.18	22.31	0.91	0.18	0.67	0.25	1.95	0.54	0.21	0.01		6.35	99.64
11	LKTD18/14	65.32	23.21	0.87	0.16	0.55	0.18	1.67	0.56	0.15	0.04		6.81	99.57
12	LKTD13/04	71.02	19.37	0.68	0.16	0.61	0.23	1.81	0.56	0.11			5.07	99.78
13	LKTD8/11	61.43	25.41	0.98	0.16	0.76	0.38	1.95	0.46	0.18	0.03		7.75	99.56
14	LKTD14/06	64.15	24.27	1.08	0.14	0.63	0.25	1.69	0.54	0.23	0.01		6.61	99.68
15	LKTD20/18	70.52	19.71	0.81	0.13	0.51	0.18	1.75	0.54	0.12			5.21	99.62
16	LKTD9A/15	66.14	22.57	0.75	0.21	0.67	0.16	1.65	0.48	0.24	0.02		6.53	99.48
17	LKTD4/17	63.43	24.52	0.71	0.16	0.78	0.42	1.87	0.5	0.34	0.01		6.86	99.67
18	LKTD28/10	68.31	21.47	0.62	0.18	0.57	0.17	1.72	0.57	0.15			5.82	99.73
19	LKTD21/07	63.68	23.79	0.91	0.16	0.7	0.42	1.93	0.52	0.3	0.04		7.12	99.61
20	LKTD25/09	62.55	25.04	1.03	0.14	0.74	0.4	1.91	0.52	0.29	0.02		7.01	99.71
21	LKTD23/19	66.22	22.89	0.77	0.16	0.59	0.23	1.69	0.5	0.19	0.03		6.27	99.6
22	LKTD13/05	62.59	23.78	1.85	0.12	0.72	0.44	1.89	0.51	0.32	0.02		7.16	99.45
23	LKTD19/13	64.83	23.77	1.28	0.18	0.65	0.16	1.63	0.46	0.27	0.01		6.28	99.6

24	LK 148T/1	62.60	24.65	1.41	0.34	0.03	0.63	0.45	0.95				7.16	98.250
25	LK 148T/6	63.12	23.63	2.45	0.32	0.12	0.02	0.91	0.99				6.86	98.420
26	LK 174 T/16	56.68	22.68	7.53	0.67	0.17	0.28	0.68	0.92				7.14	96.760
27	LK 150 T/36	68.78	19.15	1.37	0.23	0.22	0.61	0.76	0.74				4.99	96.850
28	LK 150 T/41	61.50	20.92	7.00	0.44	0.10	0.24	1.69	1.07				5.50	98.460
29	LK149 T/56	76.42	15.18	0.75	0.27	0.07	0.49	0.77	0.95				4.26	99.190
30	LK 121 T/66	56.36	27.99	1.82	0.36	0.09	0.46	0.63	1.22				8.93	97.860
31	LK 122 T/72	56.60	26.07	2.82	0.35	0.07	0.13	0.17	1.25				8.22	95.700
32	LK 122 T/77	74.52	14.94	0.91	0.28	0.09	0.29	1.10	0.86				5.31	98.540
33	LK 120 T/87	81.16	10.72	0.83	0.17	0.14	0.74	1.02	0.66				3.35	98.790
34	LK 126 T/117	64.96	18.85	3.82	0.26	0.05	0.08	1.07	0.86				5.71	95.660
35	LK 132 T/148	75.84	14.90	1.40	0.31	0.01	0.39	0.59	0.76				4.40	98.668
36	LK 156 T/154	60.86	20.75	5.76	0.39	0.03	0.12	1.02	0.97				6.20	96.168
37	LK 155 T/169	76.66	14.33	1.12	0.24	0.01	0.48	0.71	0.81				3.95	98.416
38	LK 133 T/178	59.38	23.78	3.08	0.52	0.06	0.14	0.19	0.92				6.08	94.237
39	LK 133 T/179	68.26	17.26	4.29	0.32	0.09	0.39	0.51	0.89				5.35	97.428
40	LK 163 T/214	63.60	21.84	3.15	0.42	0.01	0.19	0.91	1.60				6.80	98.599
41	LK 162 T/221	55.70	27.32	2.43	0.42	0.12	0.48	0.48	0.90				9.89	97.875
42	LK 157 T/242	63.34	21.12	2.89	0.61	0.04	0.06	1.63	1.07				6.12	96.906
43	LK 188 T/269	64.42	21.72	1.75	0.47	0.04	0.34	0.74	0.79				6.13	96.400
44	LK 175 T/285	59.56	22.95	5.88	0.99	0.46	0.08	1.00	0.79				5.55	97.260
45	LK 184 T/308	64.48	23.28	1.50	0.40	0.02	0.29	1.20	0.92				7.00	99.150
46	LK 172 T/327	73.72	14.07	3.75	0.27	0.04	0.12	1.07	0.81				4.03	97.931
47	LK 170 T/342	56.02	27.14	3.25	0.58	0.06	0.23	0.73	1.02				6.68	95.856
48	LK 170 T/344	60.24	23.49	3.50	0.52	0.02	0.08	1.10	0.84				6.56	96.418
49	LK 141 T/358	65.26	22.84	1.17	0.32	0.12	0.31	0.63	0.84				6.66	98.175
50	LK 154B T/379	57.34	26.27	2.17	0.55	0.07	0.03	1.43	0.79				7.23	95.922
51	LK 137 T/384	66.96	20.21	0.98	0.55	0.09	0.08	1.21	0.92				6.01	97.120
52	LK 137 T/388	79.50	10.32	3.48	0.20	0.03	0.47	0.70	0.76				3.38	98.874
53	LK 159 T/398	72.76	15.40	2.90	0.27	0.10	0.15	1.15	0.79				4.62	98.169
54	LK 183 T/415	67.76	16.66	3.33	0.30	0.17	0.54	1.38	0.79				5.30	96.290
55	LK 182 T/427	57.72	24.14	5.19	0.32	0.10	0.44	1.60	0.92				6.80	97.298
56	LK 179 T/432	54.04	28.38	2.96	0.45	0.14	0.71	0.54	1.15				8.54	96.987
57	LK 180 T/444	58.64	25.41	2.25	0.35	0.27	0.34	2.36	0.86				7.24	97.806
58	LK 180 T/449	59.18	23.70	4.44	0.39	0.34	0.89	1.96	0.89				6.76	98.593
59	LK 66A/457	69.12	16.89	3.57	0.49	0.04	0.57	0.87	0.86				5.29	97.720
60	LK197 T/469	84.00	9.81	0.46	0.20	0.07	0.58	0.25	0.68				3.14	99.207
61	LK191 T/474	63.58	20.01	4.50	0.37	0.25	1.05	0.15	0.92				6.12	96.972
62	LK 193 T/481	60.90	22.62	3.61	0.43	0.19	0.77	0.98	0.91				6.36	96.787
63	LK 203 T/489	60.00	23.90	2.00	0.51	0.10	0.37	1.00	0.92				7.58	96.448
64	LK 173 T/516	57.80	20.30	3.69	0.44	0.20	0.86	0.81	0.84				6.77	91.765
65	LK 200 T/524	58.70	24.58	2.46	0.32	0.28	0.73	1.21	0.97				7.38	96.673
UCC		66.55	15.39	5.04	2.48	3.59	3.27	2.80	0.64	0.15	0.10			100.00
PAAS		62.80	18.90	7.23	2.20	1.30	1.20	3.70	1.00	0.16	0.11			98.60

XRF - X-ray Fluorescence Analysis (S4- Pioneer, Bruker, Germany); wt. % - Weight percent; ppm - Parts per million
MDL - Measurement detection limit; LOI - Lost on ignition ($^{\#}$ by weight difference after ignition at 1000°C)

Chondrite-normalized REE concentrations and the calculated cerium and europium anomalies

Sample	$La/La_{chondrite}$	$Ce/Ce_{chondrtie}$	$Pr/Pr_{chondrite}$	$Nd/Nd_{chondrite}$	$Sm/Sm_{chondrite}$	$Eu/Eu_{chondrite}$	$Gd/Gd_{chondrite}$	$Tb/Tb_{chondrite}$
TRT19-08/2	160.00	114.98	85.66	62.50	33.59	17.28	23.28	20.46
TRT19-08/3	253.87	179.46	133.11	96.00	52.15	27.21	33.09	25.53
TRT19-06/1	82.02	65.13	50.93	42.65	27.05	15.08	16.98	11.51
TRT19-07/1	125.41	94.72	68.21	56.74	33.02	15.95	18.50	12.66
UCC	100.00	77.97	58.20	45.00	24.10	13.61	15.44	14.77
PAAS	123.23	98.51	72.38	56.50	28.46	14.69	17.99	16.33

Sample	$Tb/Tb_{chondrite}$	$Dy/Dy_{chondrite}$	$Ho/Ho_{chondrite}$	$Er/Er_{chondrite}$	$Tm/Tm_{chondrite}$	$Yb/Yb_{chondrite}$	$Lu/Lu_{chondrite}$	Ce/Ce*	Eu/Eu*
TRT19-08/2	20.46	18.39	17.69	18.14	17.90	17.27	17.39	0.90	0.61
TRT19-08/3	25.53	20.93	17.97	18.62	17.28	18.18	17.70	0.89	0.64
TRT19-06/1	11.51	8.34	6.42	5.71	4.60	4.08	3.55	0.95	0.69
TRT19-07/1	12.66	9.63	7.49	6.66	5.25	4.64	3.82	0.92	0.62
UCC	14.77	12.11	11.56	10.95	9.26	9.57	9.63	0.95	0.69
PAAS	16.33	14.53	13.80	13.57	12.50	13.49	13.53	0.98	0.63

Ratios of selected trace elements and other parameters related to geochemical composition of source rocks of the studied samples

Sample	LREE	HREE	∑ REE	LREE/HREE	(La/Sm)N	(Gd/Yb)N	(La/Yb)N	(La/Lu)N
TRT19-08/2	198.27	22.75	221.02	8.72	4.76	1.35	9.26	9.20
TRT19-08/3	309.71	26.65	336.36	11.62	4.87	1.82	13.96	14.34
TRT19-06/1	116.24	10.40	126.64	11.17	3.03	4.16	20.08	23.11
TRT19-07/1	165.39	11.69	177.08	14.15	3.80	3.99	27.04	32.80
UCC	133.80	14.34	148.14	9.33	4.15	1.61	10.45	10.39
PAAS	167.16	17.61	184.77	9.49	4.33	1.33	9.13	9.11

Sample	La/Sc	Th/Sc	La/Co	Th/Co	Th/Cr	Cr/Th	Co/Th	Cr/V	Y/Ni	Zr/Sc
TRT19-08/2	4.96	1.72	19.84	6.88	0.25	3.98	0.15	0.85	33.64	37.74
TRT19-08/3	5.25	1.61	12.49	3.83	0.29	3.41	0.26	0.79	5.43	14.85
TRT19-06/1	2.15	1.13	4.87	2.57	0.08	11.87	0.39	2.00	0.53	0.70
TRT19-07/1	3.05	1.18	13.63	5.29	0.10	10.37	0.19	2.13	0.97	0.20
UCC	2.21	0.75	1.79	0.61	0.11	8.76	1.65			
PAAS	2.39	0.91	1.66	0.63	0.13	7.53	1.58			

Weathering indices

No	Sample	CIA	CPA	CIW	PIA	CIA molar	ICV	A-CN-K diagram		
								Al_2O_3	$CaO + Na_2O$	K_2O
1	TRT19-08/2	89.26	98.43	97.91	97.69	8.31	0.34	0.13	0.00	0.01
2	TRT19-08/3	88.98	97.85	97.30	97.03	8.08	0.20	0.22	0.01	0.02
3	TRT19-06/1	83.23	92.47	91.12	90.19	4.96	0.31	0.24	0.02	0.03
4	TRT19-07/1	85.10	93.47	92.39	91.68	5.71	0.23	0.26	0.02	0.02
5	TRT19-8/3a	89.17	97.73	97.14	96.86	8.23	0.21	0.23	0.01	0.02
6	TRT19-8/2a	89.96	98.18	97.69	97.47	8.96	0.28	0.17	0.00	0.02
7	TRT19-10	88.20	98.25	97.25	96.93	7.48	0.24	0.14	0.00	0.01
8	LKCD4/03	89.51	98.79	94.17	93.61	6.46	0.19	0.21	0.01	0.02
9	LKCD2/01	88.34	98.40	93.78	93.14	6.03	0.21	0.19	0.01	0.02
10	LKCD2/02	88.59	98.31	93.64	93.02	6.16	0.20	0.20	0.01	0.02
11	LKTD2/16	89.59	98.85	93.67	93.06	6.23	0.34	0.19	0.01	0.02
12	LKTD7/12	90.48	98.73	89.82	89.03	5.18	0.39	0.15	0.02	0.01
13	LKTD24/08	89.42	98.47	93.85	93.31	6.55	0.22	0.22	0.01	0.02
14	LKTD7/20	88.38	98.19	93.19	92.54	5.97	0.20	0.22	0.02	0.02
15	LKTD18/14	90.63	98.74	94.71	94.29	7.48	0.17	0.23	0.01	0.02
16	LKTD13/04	87.70	98.08	92.87	92.13	5.62	0.21	0.19	0.01	0.02
17	LKTD8/11	88.32	97.60	92.68	92.07	6.17	0.19	0.25	0.02	0.02
18	LKTD14/06	90.15	98.33	93.97	93.51	7.17	0.18	0.24	0.02	0.02
19	LKTD20/18	88.80	98.52	94.16	93.57	6.32	0.20	0.19	0.01	0.02
20	LKTD9A/15	90.71	98.85	93.84	93.35	6.91	0.17	0.22	0.01	0.02
21	LKTD4/17	87.80	97.26	92.08	91.43	5.93	0.18	0.24	0.02	0.02
22	LKTD28/10	89.87	98.71	94.22	93.71	6.76	0.18	0.21	0.01	0.02
23	LKTD21/07	87.27	97.18	92.38	91.70	5.87	0.20	0.23	0.02	0.02
24	LKTD25/09	88.10	97.44	92.59	91.98	6.15	0.19	0.25	0.02	0.02
25	LKTD23/19	89.85	98.37	94.04	93.55	6.98	0.17	0.22	0.01	0.02
26	LKTD13/05	87.19	97.05	92.12	91.45	5.83	0.23	0.23	0.02	0.02
27	LKTD19/13	91.21	98.90	94.27	93.84	7.41	0.18	0.23	0.01	0.02

No	Sample	CIA	CPA	CIW	PIA	CIA molar	ICV	A-CN-K diagram		
								Al_2O_3	$CaO + Na_2O$	K_2O
28	LK 148T/1	93.98	95.97	95.76	95.68	15.62	0.15	0.24	0.01	0.00
29	LK 148T/6	95.74	99.86	98.95	98.90	19.12	0.20	0.23	0.00	0.01
30	LK 174 T/16	93.77	98.01	96.72	96.61	15.06	0.45	0.22	0.01	0.01
31	LK 150 T/36	89.59	95.02	93.17	92.89	8.60	0.21	0.19	0.01	0.01
32	LK 150 T/41	89.69	98.15	97.32	97.07	8.70	0.50	0.21	0.01	0.02
33	LK149 T/56	89.57	94.96	94.21	93.89	8.59	0.22	0.15	0.01	0.01
34	LK 121 T/66	94.59	97.37	96.82	96.74	17.47	0.16	0.27	0.01	0.01
35	LK 122 T/72	98.03	99.19	98.71	98.70	49.64	0.18	0.26	0.00	0.00
36	LK 122 T/77	89.08	96.91	95.89	95.55	8.16	0.24	0.15	0.01	0.01
37	LK 120 T/87	80.63	89.80	87.93	86.73	4.16	0.33	0.11	0.01	0.01
38	LK 126 T/117	93.18	99.31	98.83	98.76	13.65	0.33	0.18	0.00	0.01
39	LK 132 T/148	91.98	95.87	95.76	95.58	11.48	0.23	0.15	0.01	0.01
40	LK 156 T/154	93.87	99.06	98.80	98.73	15.30	0.40	0.20	0.00	0.01
41	LK 155 T/169	90.09	94.78	94.66	94.38	9.09	0.24	0.14	0.01	0.01
42	LK 133 T/178	97.76	99.04	98.59	98.58	43.63	0.21	0.23	0.00	0.00
43	LK 133 T/179	92.71	96.42	95.54	95.40	12.72	0.38	0.17	0.01	0.01
44	LK 163 T/214	94.32	98.59	98.51	98.44	16.60	0.29	0.21	0.00	0.01
45	LK 162 T/221	94.71	97.19	96.44	96.38	17.89	0.18	0.27	0.01	0.01
46	LK 157 T/242	91.60	99.53	99.19	99.12	10.91	0.30	0.21	0.00	0.02
47	LK 188 T/269	93.81	97.49	97.17	97.07	15.16	0.19	0.21	0.01	0.01
48	LK 175 T/285	94.46	99.43	95.95	95.76	11.19	0.40	0.23	0.01	0.01
49	LK 184 T/308	92.78	97.99	97.84	97.72	12.85	0.19	0.23	0.01	0.01
50	LK 172 T/327	90.78	98.62	98.12	97.95	9.85	0.43	0.14	0.00	0.01
51	LK 170 T/342	95.50	98.63	98.24	98.18	21.24	0.22	0.27	0.00	0.01
52	LK 170 T/344	94.53	99.44	99.29	99.25	17.29	0.26	0.23	0.00	0.01
53	LK 141 T/358	94.19	97.82	96.91	96.82	16.20	0.15	0.22	0.01	0.01
54	LK 154B T/379	93.84	99.81	99.33	99.29	15.23	0.19	0.26	0.00	0.02
55	LK 137 T/384	92.78	99.35	98.56	98.46	12.59	0.19	0.20	0.00	0.01
56	LK 137 T/388	86.68	93.03	92.58	92.03	6.51	0.55	0.10	0.01	0.01
57	LK 159 T/398	90.20	98.42	97.29	97.06	9.20	0.35	0.15	0.00	0.01
58	LK 183 T/415	86.09	94.94	93.29	92.68	6.19	0.39	0.16	0.01	0.01
59	LK 182 T/427	90.15	97.09	96.38	96.12	9.15	0.36	0.24	0.01	0.02
60	LK 179 T/432	93.40	96.05	95.23	95.13	14.14	0.21	0.28	0.01	0.01
61	LK 180 T/444	87.58	97.85	96.03	95.61	7.05	0.25	0.25	0.01	0.03
62	LK 180 T/449	84.93	94.18	91.92	91.20	5.64	0.38	0.23	0.02	0.02
63	LK 66A/457	89.64	94.74	94.36	94.04	8.65	0.38	0.17	0.01	0.01
64	LK197 T/469	87.89	91.14	90.07	89.82	7.26	0.23	0.10	0.01	0.00
65	LK191 T/474	89.51	92.05	90.17	90.10	8.54	0.36	0.20	0.02	0.00
66	LK 193 T/481	89.43	94.70	93.35	93.04	8.46	0.30	0.22	0.02	0.01
67	LK 203 T/489	92.73	97.52	96.80	96.65	12.76	0.21	0.23	0.01	0.01
68	LK 173 T/516	88.43	93.48	91.95	91.61	7.65	0.34	0.20	0.02	0.01
69	LK 200 T/524	89.06	95.34	93.50	93.15	8.14	0.24	0.24	0.02	0.01

CIA - Chemical Index of Alteration; Nesbitt and Young, (1982); CPA - Chemical proxy of alteration; Buggle et al., (2011); CIW- Chemical Index of Weathering; Harnois, (1988); PIA - Plagioclase Index of Alteration; Fedo et al., (1995); $CIA_{(molar)}$ - Chemical Index of Alteration expressed as CIA molar; Goldberg & Humayun, (2010); ICV - Index of Compositional Variability; Cox et al., (1995)